RESEARCH PAPER

Nanoparticle-strengthened-martensitic Surface Layered Constructed Steel by Plasma Hardening Rout

Duman Orynbekov [1]*, Tolkyn Sarsembayeva [2], Amangeldy Kanaev [2], and Alexander Gulyarenko [2]

[1] *Research and Design Laboratory for Construction and Transport Processes, L.N. Gumilyov Eurasian National University, Nur-Sultan, Kazakhstan*

[2] *Department of Standardization, Metrology and Certification, S. Seifullin Kazakh Agrotechnical University, Nur-Sultan, Kazakhstan*

ARTICLE INFO

ABSTRACT

A comprehensive study was carried out on the strain-induced martensitic transformation, its reversion to austenite, the resultant grain refinement, and the enhancement of strength and strain-hardening ability through the transformation-induced plasticity (TRIP) effect in a commercial stainless steel with emphasis on the mechanisms and the microstructural evolution. It is shown that depending on the cooling rate and temperature conditions of austenite decomposition, pearlitic and martensitic transformations proceed with the formation of gradient-layered structure, modernization of steel surface layer structure is obtained while the chemical composition, structure and the central layer properties of the processed product remain unchanged. The non-diffusive martensitic transformation is developed in the surface zone that makes the formation of needle martensite. In the underlying layers, the decomposition of austenite proceeds by diffusion and is followed by the formation of a lamellar ferrite-carbide mixture of different degrees of dispersion. It is noted that the formation in the surface layer of plasma-strengthened steel of the gradient-layered structure allows to exclude the formation of a sharp transition from martensite structures to trostite-martensite and mixed lamellar structures, which is a concentrator of internal residual stresses.

How to cite this article
Orynbekov D, Sarsembayeva T, Kanaev A, and Gulyarenko A. Nanoparticle-strengthened-martensitic Surface Layered Constructed Steel by Plasma Hardening Rout. J Nanostruct, 2021; 11(4):814-824. DOI: 10.22052/JNS.2021.02.018

INTRODUCTION

Wear processes, crack growth under static, dynamic and variable loads start from the surface, therefore, are determined by the structure and properties of a relatively thin surface layer, which plays a special role in ensuring the reliability and durability of machines and mechanisms. This fact should explain the increased interest in studies of the regularities of formation and development of gradient-layer structures after using different types of hardening thermal treatments (thermomechanical treatment, plasma, laser hardening, etc.) [1-3].

The relevance of these studies is justified by the fact that, on the one hand, the physical nature of complex processes occurring during the formation and development of gradient-layered structures has not been studied sufficiently, on the other hand, gradient-layered structures in metallic materials give steels and alloys new, previously

* *Corresponding Author Email: du.th90@yahoo.com*

unknown, properties [4,5].

Gradient-layered structures are of particular interest in surface plasma hardening. This is due to the fact that, in many cases, local heat treatment is technically and economically justified, when only the most stressed working surface of the part is hardened while retaining its original properties in the inner layers [6]. Local heat treatment is of great interest because cooling during plasma hardening proceeds at a high rate due to the small volume of heated metal, which provides hardening with only one heat transfer to the cold areas of the product without supplying the heated surface with coolant. This has an important practical value, because the process of hardening without water supply to the hardened product significantly simplifies the technological process of heat treatment [7,8].

MATERIALS AND METHODS

In order to study the specific features of formation of the layered structure in the hardened layer, special experiments aimed at finding out the effect of the layered-gradient structure in structural steel on wear resistance and resistance to brittle fracture were carried out. The study was carried out on structural steel samples with surface plasma hardening of the ridge banding. The macroscopic studies were carried out on a transverse temple with ridge height of 28 mm

after etching with 50% aqueous solution of sulfuric acid. The width of the hardening band was 30 mm, and the maximum depth of the hardening zone was 1.9 mm. Metal microstructure was studied using optical research microscope Axio Observer D1m Carl Zeiss designed to analyze the phase composition and structural features of the processed steel at a magnification of x100 to x1000. Electron microscopic studies were carried out on an electron microscope JEOLJEM 2110 at a magnification of x5000. The main advantages of the method are the possibility to study fine structure details and visual perception of the complex real structure of the treated steel. Measuring of microhardness of the hardened layer was carried out on microslips cut in cross direction from the segment with the requirement of keeping the hardened layer on the hardness tester PMT-3 at the load of 1,962N (200gs) according to the requirements of GOST 9450-2006 "Measuring of microhardness by indentation of diamond points [9].

This device provides the possibility to select the microstructure area where the indentation will be made. Due to the small size of the imprint, the microhardness of the individual phase and structural components of the steel was measured. A diamond pyramid with a square base and an angle of 136° at the base was used as an indenting

Table 1. Changes in microhardness by depth of the hardened layer.

Height from surface, mm	Microhardness, HV_{02}	Microstructure	Height from surface, mm	Microhardness, HV_{02}	Microstructure
0,05	871	Martensite	0,80	557	Sorbitol + perlite
0,10	850		0,95	553	
0,15	847		1,10	541	
0,20	802		1,25	427	
0,25	760	Troostite-martensite	1,40	427	
0,30	685		1,55	372	Perlite
0,40	628		1,70	343	
0,50	615	Troostite-sorbitol	1,90	322	
0,60	613		2,10	295	Perlite + Ferrite
0,70	585		2,30	295	

tool (indenter). Based on the measured diagonal of the indentation, the hardness value is calculated as the ratio of the applied load divided by the surface of the obtained imprint. To exclude possible roughness of the edge surface during grinding and polishing on the value of microhardness when measuring microhardness of the sample, the first indentation was applied at a distance of not less than 0.05 mm from the surface. For plotting of dependence diagram of microhardness on section of the hardened layer microhardness was measured according to GOST 9450 separately on not etched samples. The chemical composition of steel in the depth of plasma hardening and the non-hardened zone was analyzed on a Leica Microsystems SPECTROLABJrSSD spark spectrometer [10].

RESULTS AND DISCUSSION
Characterization

The conducted metallographic studies show that during high-speed heating and cooling, during plasma hardening, a gradient-layered (mixed) structure is formed in the surface area of the processed product. Microhardness values are given in Table 1. As can be seen from the table, the change of microhardness occurs in the range from 871 HV_{02} to 295 HV_{02}. At a depth of 0,05 - 0,20 mm it is observed martensitic structure with microhardness 871 - 802 HV_{02}, at a depth of 0,25 - 0,60 mm troostite-martensitic structure with microhardness 760 - 613 HV_{02}, then troostite-sorbite structure at a depth of 0,70 - 1,10 mm with microhardness 585 - 541 HV_{02}, sorbite-perlite at depth 1,25 -1,90 mm with microhardness 427 - 322 HV_{02} followed by a gradual transition to the

initial ferrite-perlite structure with microhardness ~ 295 HV_{02}.

The SEM images obtained from the cold rolled samples at room temperature to strain of 0.1 and 1.1 are shown in Fig. 1 as the candidates of low and high straining conditions. Fig. 1 a shows the SEM image of a heavily rolled sample to strain of 1.1, depicting the morphology of the DIM. Moreover, as shown in Fig. 1 b, the presence of ε-martensite is signified by XRD pattern of slightly cold rolled sample to strain of 0.1.

Changes in the microstructure of steel treated by surface plasma hardening are shown in Fig. 2. The formation of several structural zones of different microhardness is clearly observed along the depth of hardening. On the surface there is a zone whose chemical composition corresponds to the composition of steel with carbon content of 0.63 %. At shock cooling the transformation of austenite into needle martensite with dispersity of 5-15 microns takes place. The zone of austenite transformed in the solid state into trostite-martensite follows. In the microstructure of these layers the presence of a small amount of residual austenite is observed, the amount of which varies and depends on the depth of the hardened layer.

Next comes a layer of troostite-sorbitol, where the microhardness decreases and depends on the volumetric content of the presented phases, then sorbitol and pearlite appear in the structure. The area of the appearing sorbitol is determined by the central areas of the former austenitic grains and is characterized by less dispersion of the ferrite and cementite components in them as compared to troostite and has a lower microhardness [11, 12]. The microhardness in this zone also depends
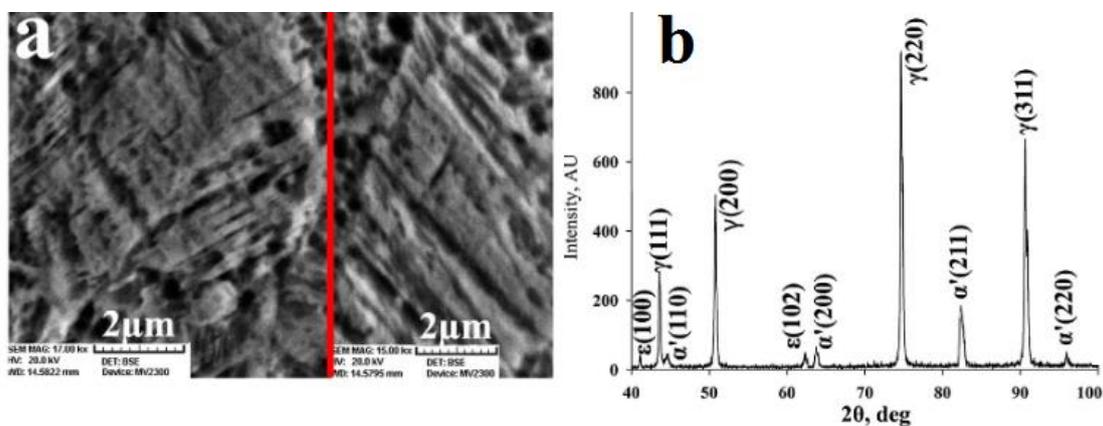

Fig. 1. SEM images illustrating (a) the morphology of martensite and (b) XRD pattern of slightly cold sample to strain of 0.1.

on the volume amount of phases present. Then, with deepening inside the sample, ferrite appears at the interface of the former austenitic grains and its quantity gradually increases. The structure smoothly transforms into a ferrite-pearlite structure. The total microhardness decreases to the initial one (290-295 HV02). The initial structure is a mixture of ferrite and pearlite grains with the volume fraction of each phase respectively 40-60 %.

The change in microhardness along the cross-section of the hardened zone (Fig. 3) shows the layered (inhomogeneous) structure after surface plasma hardening, which provides the product with high mechanical and operational properties. In this regard, it is appropriate to note that while recently (at the end of the twentieth century) the widespread requirement for a homogeneous structure seemed reasonable and obvious, at present, in many cases the presence of a non-uniform gradient structure allows the material to acquire new, previously unknown, properties. In this case, the optimal structure of metal from the position of providing the required set of mechanical properties (strength, hardness, ductility and impact toughness) can be highly dispersed martensite, martensitic-troostite and troostite-sorbit [13, 14].

We note that the above structural features after plasma treatment are explained by ultra-high heating and cooling rates, unattainable with traditional methods of heat treatment. This leads to the fact that the structural and phase components of steel after plasma treatment (austenite, martensite, troostite, sorbitol) are characterized by increased dispersion and a higher level of internal (phase and structural) residual stresses of type 11, as well as pronounced chemical microheterogeneity [15-17].

As noted above, at superfast heating rates, phase transformations shift to high temperatures. This fact strongly affects the kinetics of emergence and growth of new phase beginnings. Therefore, it follows that by regulating the amount of input energy it is possible to create such conditions of ($\alpha \rightarrow \gamma$) transformation, when the only possibility of transition of initial phases into austenite is the process of phase generation. This opens the possibility of obtaining ultra-fine austenite, when the grain size will be proportional to the critical size under the temperature achieved in the process of high-temperature high-speed heating.

To experimentally verify these statements, we carried out special studies to determine the chemical composition of the alloy with excitation of the spectrum in a spark on a spark spectrometer
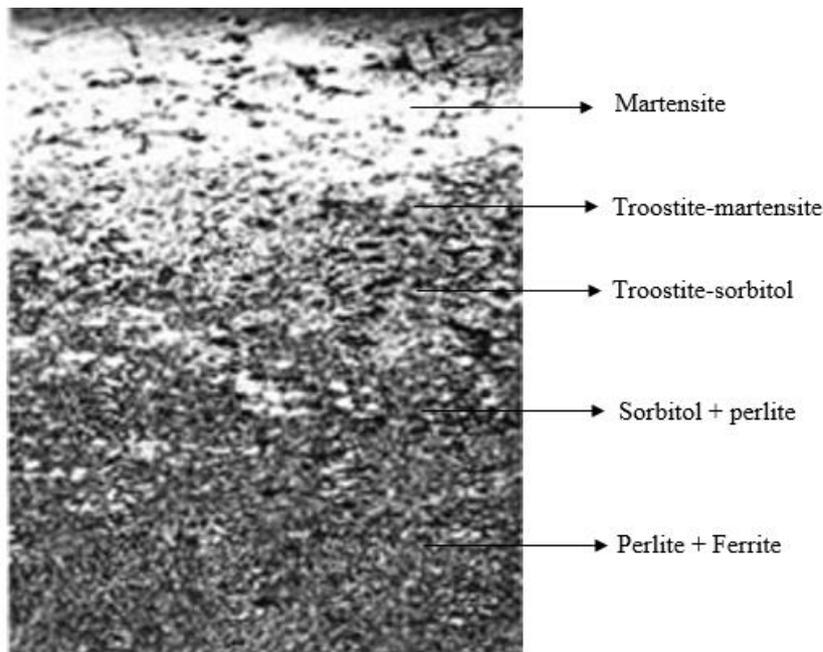

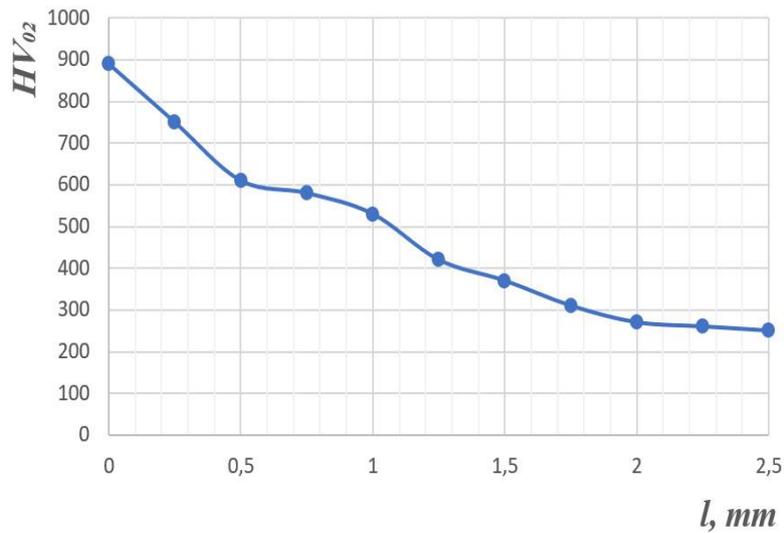Fig. 2. Gradient-layered structure of the bandage ridge in the hardened zone.

Fig. 3. Microhardness curve along the hardened zone cross section.

SPECTROLABJrSSD of Leica Microsystems. The data of chemical analysis on the depth of plasma hardening and the non-hardened zone presented in Table 2 confirm the chemical micro heterogeneity of structural and phase components of the analyzed steel.

It can be seen that the carbon content along the depth of the hardened zone varies from 0.002 to 0.06 % (at). The same micro heterogeneity in the depth of the hardened zone has other stable steel

Table 2. Chemical composition data by depth of plasma hardening and non-hardened zone.

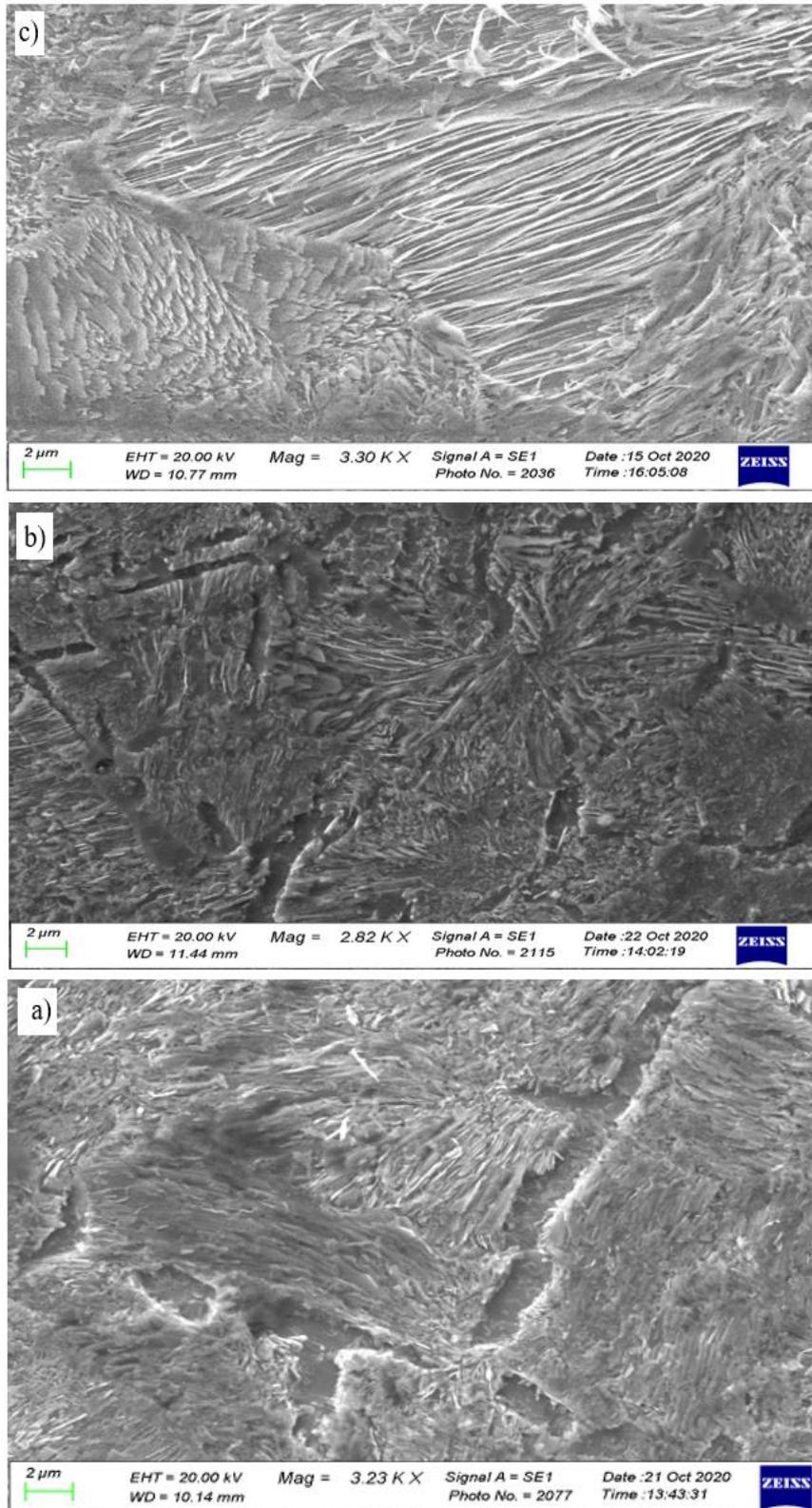| Name of zones by depth of hardening	Chemical composition, % (ат.)								
	C	Si	V	Mn	Fe	W	Ti	Cr	S
1	2	3	4	5	6	7	8	9	10
t 2	0,06	0,002	-	0,063	0,855	0,008	-	-	-
t 3	0,5	0,002	0	0,06	0,87	0,02	0,0002	-	0,0005
t 4	0,002	-	0,001	0,065	0,87	0,009	-	0,001	0,002
t 5	0,05	0,0005	0,001	0,062	0,86	0,018	0,004	-	0,002
t 6	0,047	0,0035	-	0,072	0,87	-	-	0,001	-
t 7	0,035	0,004	-	0,068	0,89	0,002	0,0026	-	-
t 8	0,02	0,0018	0,0027	0,07	0,88	0,019	-	-	-
t 9	0,027	0,0025	0,0023	0,065	0,88	-	-	-	-
t 10	0,03	0,004	-	0,074	0,86	0,026	-	-	-
t 11	0,04	0,004	0,001	0,069	0,88	-	0,003	-	
Basis	0,008	-	-	0,059	0,90	-	-	-	

Fig. 4. Structure of the products of austenite decomposition during continuous cooling (a - troostite-martensite, 630-760, HV$_{02}$); (b- troostite-sorbitol, 585-615 HV$_{02}$, c- sorbitol + perlite, 557-427 HV$_{02}$).

impurities (Si, Mn, V, etc.).

At heating parameters (t ≈ 5000 0C) and cooling rate (Vohl ≈ 30000C/s), typical for plasma treatment, processes related to homogenization of liquid and solid solutions do not have time to complete in the volume of individual grains. It promotes creation of nonequilibrium metastable structures of high hardness with good resistance to wear and microseizure during friction [18, 19].

It should be noted that the process of structure formation during hardening after exposure to highly concentrated energy flows follows the general laws of structure formation described by the phase equilibrium diagram of iron-carbon (Fe-C). The depth of hardened structural zones under plasma action depends on the heating parameters and is determined by the mechanism and kinetics of phase transformations in nonequilibrium states [20,21].

The two-phase structure of sorbitol and troostite is identified only under an electron microscope, since the interlayer distance between these structures is at the limit of optical microscope resolution (~0.2 μm). Therefore, Fig. 4 shows photos of sorbitol and troostite, respectively, taken with an electron microscope at a magnification of x5000. It is clearly seen that both these structural components consist of interlaced plates of ferrite and cementite.

It is important to emphasize that during continuous cooling it is not possible to distinguish the processes of formation of pure troostite, sorbitol or pearlite, as the rate of temperature change along the section of the cooled product does not remain constant, it is variable and changes according to a certain law, depending on the thermophysical properties of steel [22, 23]. In fact, the transformation processes may overlap one another in terms of temperature and time of their development. This leads to the formation of mixed structures in the form of martensite + troostite, troostite + sorbitol or sorbitol + perlite (Fig. 4).

According to Fig. 5, we can assume that the kinetics and patterns of formation of gradient-layered structure based on a typical thermokinetic diagram of pre-eutectoidal carbon steel (0.59-0.63%C) is the analogue of the studied steel. The solid lines correspond to the decay of austenite at continuous cooling (thermokinetic), the dotted lines to the decay of austenite at constant temperature (isothermal) [24, 25].

It can be seen from Fig. 5 that the thermokinetic diagram at temperatures above the martensitic point Mn (~260 °C) is characterized by only one kinetic maximum, which means that there is no intermediate mechanism of austenite decomposition (unshaded part of the diagram).
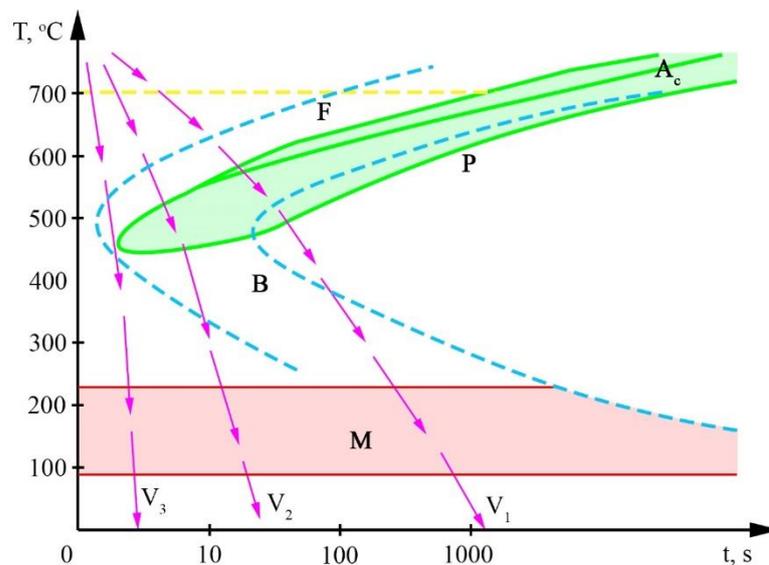

Fig. 5. The scheme of the diagram of supercooled austenite decomposition of pre-eutectoidal (0.60-0.65% C) structural steels. Dashed lines are corresponded to isothermal transformation of austenite, solid lines to transformation at continuous cooling (thermokinetic diagram).

At temperatures above this maximum, the decomposition of austenite proceeds by diffusion and is characterized by the formation of a ferrite-carbide mixture of varying degrees of dispersion. Depending on the degree of dispersion, the ferrite-carbide mixture is called pearlite, sorbitol, or troostite, or coarse-, medium-, and fine-dispersed pearlite, respectively [26-28].

Fig. 5 shows that when austenite is cooled at speed V3 (critical hardening speed) and above, lamellar martensite is formed. At lower cooling rate V2, supercooled austenite transforms into troostite-martensite partly by the pearlitic (diffusion), partly by the martensitic (non-diffusion) mechanism. At even lower cooling rates V1 the transformation develops by the diffusion mechanism with the formation of troostite and sorbitol.

At the same time, the thermokinetic diagram clearly shows that the intermediate mechanism of austenite transformation with the formation of bainite structures cannot be realized, because the transformation in this case develops either by the pearlitic mechanism (cooling rates V1 and below), or by the mixed pearlite-martensite mechanism (cooling rates between V1 and V2), or by the martensitic mechanism (cooling rates V3 and above).

Note that both pearlitic and martensitic transformations are based on the polymorphic transition ($\gamma \rightarrow \alpha$) of the face-centered austenite crystal lattice into the volume-centered lattice of equilibrated or supersaturated ferrite [29, 30].

A comparison of the kinetics of austenite transformation under isothermal conditions and during continuous cooling shows that the corresponding lines in the thermokinetic diagrams are on the right and below the analogous lines of the isothermal diagram. This indicates that the stability of supercooled austenite under continuous cooling is somewhat greater and the transformation proceeds at lower temperatures than in the case of isothermal decomposition of supercooled austenite [31].

In practical terms, this is reflected in the interlayer spacing, which is the most important mechanical characteristic of structural steels. The interlayer spacing is the averaged sum of the thicknesses of two neighboring plates of ferrite and cementite pearlitic structures. The higher the cooling rate, the lower the interlayer spacing and the more dispersed the resulting ferrite-carbide mixture, the higher the microhardness (hardness) of the steel [32].

When analyzing the structural transformations, it should be kept in mind that the division of ferrite-cementite structures into pearlite, sorbitol, or troostite is conditional and there is usually no clear boundary between these structures. This is explained by the fact that in practice it is not possible to distinguish the processes of formation of pure troostite, sorbitol or perlite, since the rate of temperature change along the section of the cooled product in the process of continuous cooling does not remain constant. As noted above, it is variable and varies according to a certain law
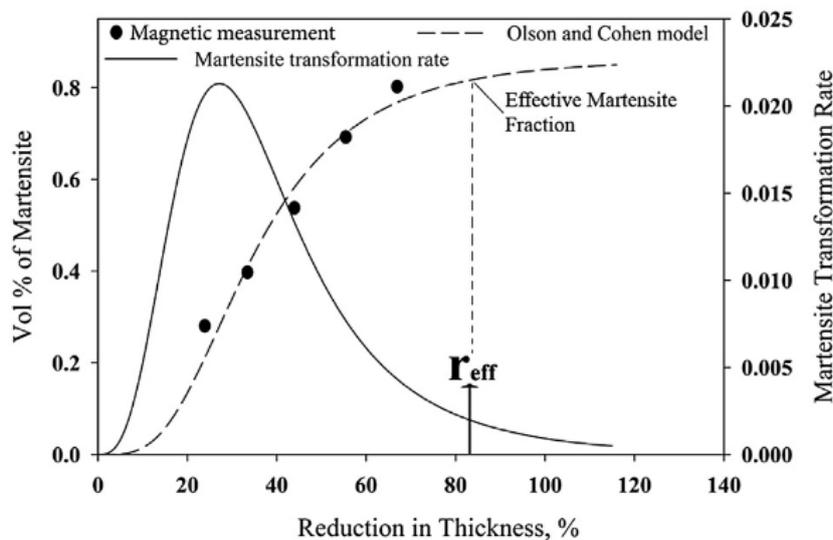

Fig. 6. Introducing the effective reduction in thickness and the corresponding martensite fraction.

that depends on the thermal properties of steel [33, 34].

Moreover, unlike pearlite, sorbitol and troostite are not equilibrium structures, since in real production conditions cooling is usually non-uniform and this leads to a certain saturation of sorbitol and troostite ferrite with carbon, which naturally affects the mechanical properties. In particular, the mechanical properties of steel with pearlite, sorbitol or troostite structures are directly proportional to the interface area between ferrite and cementite. Therefore, as the austenite decomposition temperature decreases and the structure is refined (the degree of dispersion increases), the ferrite plates become somewhat oversaturated with carbon, the strength characteristics (strength -σ_v hardness - HB) increase, and the plastic characteristics (relative elongation - δ and contraction -ψ) decrease [35].

The microstructures shown in Fig. 2 illustrate the superimposition of martensitic transformation on pearlitic transformation. Thus, at cooling rate V2 in the temperature range ~ 550 °C - 460 °C some part of austenite by diffusion mechanism turns into troostite, the remaining part below the point Mn (~260 °C) turns into martensite without diffusion. These and other similar examples show that the experimental study of structure formation processes during variable rate cooling is a difficult task. Depending on a number of factors and, primarily, on the cooling rate, the kinetics and temperature conditions for the development of a particular transformation may vary within certain limits.

Therefore, it is not always possible to outline temperature boundaries, in which the transformation proceeds only by one mechanism (perlite-diffusion, intermediate or martensite-no-diffusion) and clearly distinguish structural zones of formation of troostite, sorbitol or pearlite. In reality, the processes of supercooled austenite transformation can overlap one another in temperature and time of their development, which leads to the formation of mixed plate-type structures [36].

Fig. 6 reveals that after a certain range of reduction in thickness, the rate of DIMT dramatically drops, which is a typical observation for DIMT. The study of thetransformation rate isrequired to characterize this fact. The required plot is also depicted in Fig. 6. A realistic estimate is to consider the reduction in thickness corresponding to the 10% of the maximum transformation rate as the effective reduction in thickness. It is obvious that reff and its corresponding martensite fraction (effective martensite fraction) can be considered as the reasonable parameters in studies dedicated to production of DIM.

CONCLUSION

In the present study, the mechanism and kinetics of structure formation of plasma-strengthened structural steel change depending on the cooling rate and temperature conditions for the development of the austenitic-martensitic transformation was investigated. The data indicated that as the cooling rate increases, the austenite transformation, which is based on a shear phase transition ($\alpha \rightarrow \gamma$) shifts downward on the temperature scale. The higher the cooling rate, the more dispersed the resulting ferrite-carbide mixture, the smaller the plate spacing. Therefore, as the degree of dispersion increases, the strength characteristics increase and the plastic characteristics decrease.

Besides, it was found that the formation of gradient-layered structure in the surface layer of plasma-strengthened steel allows to exclude formation of sharp border of transition from martensite structures to troostite-martensite and mixed lamellar structures which is the concentrator of internal residual stresses. This is one of the main factors increasing the contact-fatigue strength of steel and contributing to its crack resistance.

ACKNOWLEDGMENT

CONFLICT OF INTEREST

The authors declare that there is no conflict of interests regarding the publication of this manuscript.

REFERENCE

1. Brownlie F, Anene C, Hodgkiess T, Pearson A, Galloway AM. Comparison of Hot Wire TIG Stellite 6 weld cladding and lost wax cast Stellite 6 under corrosive wear conditions. Wear. 2018;404-405:71-81.
2. Abbasi E, Luo Q, Owens D. Case study: Wear mechanisms of NiCrVMo-steel and CrB-steel scrap shear blades. Wear.

2018;398-399:29-40.

3. Cole-Filipiak NC, Knepper R, Wood M, Ramasesha K. Sub-picosecond to Sub-nanosecond Vibrational Energy Transfer Dynamics in Pentaerythritol Tetranitrate. The Journal of Physical Chemistry Letters. 2020;11(16):6664-6669.

4. Wu XL, Yang MX, Yuan FP, Chen L, Zhu YT. Combining gradient structure and TRIP effect to produce austenite stainless steel with high strength and ductility. Acta Materialia. 2016;112:337-346.

5. Mamina LI, Gilmanshina TR, Anikina VI, Baranov VN, Lytkina SI, Abkaryan AK, et al. Influence of Activation Time on Parameters of Graphite Structure. Izvestiya Vuzov Poroshkovaya Metallurgiya i Funktsional'nye Pokrytiya (Proceedings of Higher Schools Powder Metallurgy and Functional Coatings). 2015(3):21.

6. Kanayev AT, Bogomolov AV, Kanayev AA. Increase of Wear Resistance and Contact-Fatigue Strength of Wheel Steel by Plasma Hardening. Solid State Phenomena. 2018;284:1144-1150.

7. Yim D, Sathiyamoorthi P, Hong S-J, Kim HS. Fabrication and mechanical properties of TiC reinforced CoCrFeMnNi high-entropy alloy composite by water atomization and spark plasma sintering. Journal of Alloys and Compounds. 2019;781:389-396.

8. Praveen S, Bae JW, Asghari-Rad P, Park JM, Kim HS. Annealing-induced hardening in high-pressure torsion processed CoCrNi medium entropy alloy. Materials Science and Engineering: A. 2018;734:338-340.

9. Using the GOST 28147-89, GOST R 34.11-94, GOST R 34.10-94, and GOST R 34.10-2001 Algorithms with Cryptographic Message Syntax (CMS). RFC Editor; 2006 2006/05.

10. Chen X, Gao J, Liu C, Zhao Y. Effect of neutralization on the setting and hardening characters of hemihydrate phosphogypsum plaster. Construction and Building Materials. 2018;190:53-64.

11. Bayatanoval.B BBea, et al. Internal Stresses and Dislocation Structure of Low-Carbon Steel after Electrolyte-Plasma Nitrocementation. International Journal of Mechanical and Production Engineering Research and Development. 2020;10(3):14493-14502.

12. Kanayev AT, Jaxymbetova MA, Kossanova IM. QUANTITATIVE ASSESSMENT OF THE YIELD STRESS OF FERRITE-PEARLITIC STEELS BY STRUCTURE PARAMETERS. Series of Geology and Technical Sciences. 2021;447(3):65-71.

13. Vander Voort G. Microstructure of Ferrous Alloys. Analytical Characterization of Aluminum, Steel, and Superalloys: CRC Press; 2005. p. 157-234.

14. Mottahedi AA. Investigation of Phase Transformation of Forged Steel Cold Rolls due to Heat Affecting and Prevent its Failure. Defect and Diffusion Forum. 2009;289-292:219-224.

15. Zadorozhny RN, Romanov IV. Increasing the wear resistance of the working bodies of agricultural machines with secondary carbide materials. Strengthening Technologies and Coatings. 2022:24-27.

16. Application of Electrolytic Plasma Process in Surface Improvement of Metals: A Review. Letters in Applied NanoBioScience. 2020;9(3):1249-1262.

17. Jones BJ, Anguilano L, Ojeda JJ. Argon plasma treatment techniques on steel and effects on diamond-like carbon structure and delamination. Diamond and Related Materials. 2011;20(7):1030-1035.

18. Li X, Zhang Z, Cheng X, Huo G, Song Q, Xu Y. Direct achievement of ultra-high strength and good ductility for high Co-Ni secondary hardening steel by combining spark plasma sintering and deformation. Materials Letters. 2021;290:129465.

19. Rahadilov BK, Zhurerova LG, Sagdoldina ZB, Kenesbekov AB, Bayatanova LB. Morphological Changes in the Dislocation Structure of Structural Steel 20GL after Electrolytic-Plasma Hardening of the Surface. Journal of Surface Investigation: X-ray, Synchrotron and Neutron Techniques. 2021;15(2):408-413.

20. Linnik VA, Onegina AK, Andreev AI, Aldarkin KK, Sinaiskii VM, Grigorenko LP. Surface hardening of steels by plasma hardening. Metal Science and Heat Treatment. 1983;25(4):241-245.

21. Korotkov VA. Strengthening of Steel by Plasma Quenching and Carbonitriding. Russian Engineering Research. 2019;39(3):234-236.

22. Shtayger MG, Kondratiev VV, Balanovsky AE, Karlina AI, Govorkov AS. APPLICATION OF SCANNING ELECTRONIC MICROSCOPY FOR METALLOGRAPHY OF WELDED JOINTS OF RAILS. Proceedings of the International Conference "Aviamechanical engineering and transport" (AVENT 2018): Atlantis Press; 2018.

23. Kuteneva S, Gladkovsky S, Dvoynikov D, Segreev S. Microstructure and brittle fracture resistance of layered steel composites produced by explosion welding and pack rolling followed by heat treatment. Letters on Materials. 2019;9(4):442-446.

24. Mitrović V. Resilience: detecting vulnerability in marginal groups. Disaster Prevention and Management. 2015;24(2):185-200.

25. Kokawa H. Weld decay-resistant austenitic stainless steel by grain boundary engineering. Journal of Materials Science. 2005;40(4):927-932.

26. Wright WW. Materials science and engineering. An introduction 2nd Edition W. D. Callister, Jr John Wiley & Sons, New York, 1991. pp. xxi + 791, price E53.00. ISBN 0-471-50488-2. Polymer International. 1993;30(2):282-283.

27. Sánchez-Alarcos V, Recarte V, Khanna DLR, López-García J, Pérez-Landazábal JI. Deformation induced martensite stabilization in Ni45Mn36.7In13.3Co5 microparticles. Journal of Alloys and Compounds. 2021;870:159536.

28. El-Sesy IA, Klaar H-J, Hussein A-HA. Effect of intercritical temperature and cold-deformation on the kinetics of austenite formation during the intercritical annealing of dual-phase steels. Steel Research. 1990;61(3):131-135.

29. Yahyaoui H, Sidhom H, Braham C, Baczmanski A. Effect of interlamellar spacing on the elastoplastic behavior of C70 pearlitic steel: Experimental results and self-consistent modeling. Materials & Design. 2014;55:888-897.

30. Popova NA, Nikonenko EL, Tabieva EE, Uazyrkhanova GK, Gromov VE. Influence of surface quenching on morphology and phase composition of ferritic-pearlitic steel. Izvestiya Ferrous Metallurgy. 2021;63(11-12):915-921.

31. Yang X, Yu W, Tang D, Shi J, Li Y, Fan J, et al. Effect of Cooling Rate and Austenite Deformation on Hardness and Microstructure of 960MPa High Strength Steel. Science and Engineering of Composite Materials. 2020;27(1):415-423.

32. Xiong Y, He TT, You L, Li PY, Chen LF, Ren FZ, et al. Microstructure and microhardness of pearlitic steel after laser shock processing and annealing. Materials Science and Technology. 2015;31(15):1825-1831.

33. Bogomolov AV, Kanaev AT, Sarsembaeva TE. Determination of Mechanical Characteristics Plasma Hardened Wheel Steel. IOP Conference Series: Materials Science and Engineering. 2020;969(1):012037.

34. Brover AV, Brover GI, Moysova OB. Transformation of the structure and properties of materials at laser-acoustic processing. Materials Today: Proceedings. 2021;38:1592-1594.

35. Liu K, Jiang Z, Li J. Study on Troostite Structures of Grey Cast Iron Processed by Heat Treatment. Procedia Engineering. 2011;15:4387-4391.

36. Moreno M, Teixeira J, Ghanbaja J, Bonnet F, Allain S. Evolution of cementite composition along the processing of cold-rolled and annealed Dual-Phase steels. Materialia. 2019;6:100179.